PHYSICAL REVIEW D VOLUME 17, NUMBER 3 1 FEBRUARY 1978

Inclusive neutral-strange-particle production in $\pi^- p$ interactions at 15 GeV/c

F. Barreiro, O. Benary,* J. E. Brau, J. Grunhaus,† E. S. Hafen, R. I. Hulsizer, U. Karshon,‡ V. Kistiakowsky, T. Lainis, A. Levy,† P. A. Miller, A. Napier, I. A. Pless, J. P. Silverman, P. C. Trepagnier, J. Wolfson, and R. K. Yamamoto

Laboratory for Nuclear Science, Massachusetts Institute of Technology, Cambridge, Massachusetts 02139

(Received 25 July 1977)

A study of the inclusive production of K_S^0, Λ, and $\bar{\Lambda}$ in $\pi^- p$ interactions at 15 GeV/c is presented. Inclusive cross sections for single neutral strange particles and neutral-strange-particle pairs are given. Longitudinal- and transverse-momentum distributions of the produced particles are presented. The average charged multiplicities of the systems recoiling against the Λ and the K_S^0 are compared and the results analyzed in the framework of a simple model. The Λ polarization is found to be in good agreement with Λ production from other strangeness-nonannihilating processes. Prŏduction of Λ's in the target fragmentation region is studied in the framework of the triple-Regge-pole-exchange model. The cross section for inclusive $K^{*+}(890)$ production has been measured as 195 ± 35 μb, and the $\Sigma^+(1385)$ inclusive cross section has been found to be 174 ± 25 μb. The $K^{*+}(890)$ and $\Sigma^+(1385)$ differential cross sections as functions of rapidity and transverse momentum are presented and discussed.

I. INTRODUCTION

The inclusive production of pions in hadron-hadron collisions has been extensively investigated in the last decade. In contrast, little has been done with charged-strange-particle production in πN and NN collisions since the cross sections for associated production are small and the identification of $K^\pm$ at medium and high energies is difficult. Inclusive neutral-strange-particle production can be investigated more easily since one has the obvious advantage of unique detection by visual techniques (e.g., bubble chambers) and almost unambiguous identification from decay kinematics. Several papers have been published recently on inclusive production of K_S^0, Λ, and $\bar{\Lambda}$ in $\pi^\pm p$ and pp interactions.[1] Also, several $\pi^\pm p$ experiments in the Fermilab momentum range (100–250 GeV/c) are currently being analyzed for neutral-strange-particle production.[2]

In this paper results are presented on the following inclusive reactions at 15 GeV/c:

$$\pi^- p \to K_S^0 + X\,, \tag{1}$$

$$\to \Lambda + X\,, \tag{2}$$

$$\to \bar{\Lambda} + X\,. \tag{3}$$

Reactions (2) and (3) include Λ ($\bar{\Lambda}$) produced both directly in $\pi^- p$ interactions and as the $\Sigma^0(\bar{\Sigma}^0)$ decay products.

Results are also presented for the inclusive reactions:

$$\pi^- p \to K_S^0 \Lambda + X\,, \tag{4}$$

$$\to \Lambda\bar{\Lambda} + X\,, \tag{5}$$

$$\to K_S^0 \bar{\Lambda} + X\,, \tag{6}$$

$$\to K_S^0 K_S^0 + X\,. \tag{7}$$

The experimental details and processing procedures are described in Sec. II. Cross sections for reactions (1)–(7) are presented in Sec. III and compared to results of other $\pi^\pm p$ experiments. In the same section, inclusive distributions of the neutral strange particles are given as functions of the center-of-mass production angle, invariant Feynman x, rapidity, and transverse momentum squared P_T^2. The average charged multiplicity of the system recoiling against the Λ (K_S^0) as a function of the recoiling system's invariant mass squared is also presented and discussed in Sec. III. In Sec. IV the polarization of the Λ particles is studied and Λ production is analyzed in the framework of a triple-Regge model. Finally, resonances that decay into a V^0 and charged pions are investigated, and the results are presented in Sec. V. A summary of the results and the conclusions are given in Sec. VI.

II. EXPERIMENTAL PROCEDURE

The data for the present study are taken from an exposure of about 470 000 pictures taken in the SLAC 82-in. hydrogen bubble chamber exposed to a 15-GeV/c π^- beam. About 200 000 events (corresponding to about 8.2 events per μb) have been scanned. Part of the film was double scanned for all events with at least one visible V^0, in order to calculate the scanning efficiency for each topology.

This study is based on about 9500 events in which one or more neutral decays (V^0's) were associated with the production vertex. All of these events were measured by the MIT PEPR (Precision Encoding and Pattern Recognition) system and processed through the geometry program GEOMAT.[3] After geometrical reconstruction, all V^0's were processed through the kinematical-fitting program SQUAW,[4] where fits were attempted to the following decay hypotheses:

$$K_S^0 \to \pi^+\pi^- , \tag{8}$$

$$\Lambda \to p\pi^- , \tag{9}$$

$$\bar{\Lambda} \to \bar{p}\pi^+ , \tag{10}$$

$$\gamma p \to e^+e^-p . \tag{11}$$

Although most of the V^0's yielded a three-constraint (3C) fit in which the neutral particle was required to come from the primary vertex of the interaction, about 10% received only a 1C fit. These latter events are primarily the result of either elastic scattering after production but before decay, or association of the V^0 with the wrong primary vertex by the scanner. Since such events would contaminate inclusive distributions, only events with 3C fits were included in the following analysis.

To investigate possible electron pair contamination remaining in the data after V^0's uniquely fitting hypothesis (11) were removed from the sample, the decay tracks of the V^0's were assumed to be electrons, and the distributions of the unfitted invariant mass $M(e^+e^-)$ were calculated. In all such distributions a pronounced peak was found near $M(e^+e^-)=0$. Events with $M(e^+e^-) \leq 30$ MeV were rejected from the sample in order to remove electron pairs misidentified as V^0's.

Using this cut together with a fiducial volume cut and a cut on the minimum distance between the primary vertex and decay vertex of 0.5 cm, and accepting only those fits with $\chi^2 < 18$, a sample of 6134 3C events was obtained in which at least one neutral strange particle has been detected via its decay (8), (9), or (10). About 15% of these remaining 3C fits are ambiguous, i.e., more than one decay hypothesis yielded an acceptable fit. The distribution of fits according to hypothesis is shown in Table I.

The invariant mass of the decay particles has been plotted as $M(p\pi^-)$ for unambiguous K_S^0 fits [the unshaded area of Fig. 1(a)]. A sharp dip occurs at the Λ mass since by definition such events will be ambiguous if they point back to the primary vertex. A similar effect occurs when the unique Λ events [Fig. 1(b)] or the few $\bar{\Lambda}$ events (not shown) are plotted as $M(\pi^+\pi^-)$ and when unique K_S^0 events are plotted as $M(\bar{p}\pi^+)$. The correct assignment of the ambiguous events should fill in these dips.

To resolve the ambiguities, the following algorithm was used. For $K_S^0/\bar{\Lambda}$ ambiguities, the V^0

TABLE I. Number of events after kinematical fit of V^0 (3C only) (after cuts; see text).

	Events	Weighted events[a]
Unique K	3711	4205
Unique Λ	1873	2084
Unique $\bar{\Lambda}$	69	80
Ambiguous K/Λ	800	...
Ambiguous $K/\bar{\Lambda}$	162	...
Ambiguous $\Lambda/\bar{\Lambda}$	0	...
Ambiguous $K/\Lambda/\bar{\Lambda}$	1	...
Resolved K	3994	4523
Resolved Λ	2528	2850
Resolved $\bar{\Lambda}$	94	111
$\Lambda\bar{\Lambda}$	20	26
$K\bar{K}$	175	224
$K\Lambda$	282	359
$K\bar{\Lambda}$	4	6

[a] By escape probability.

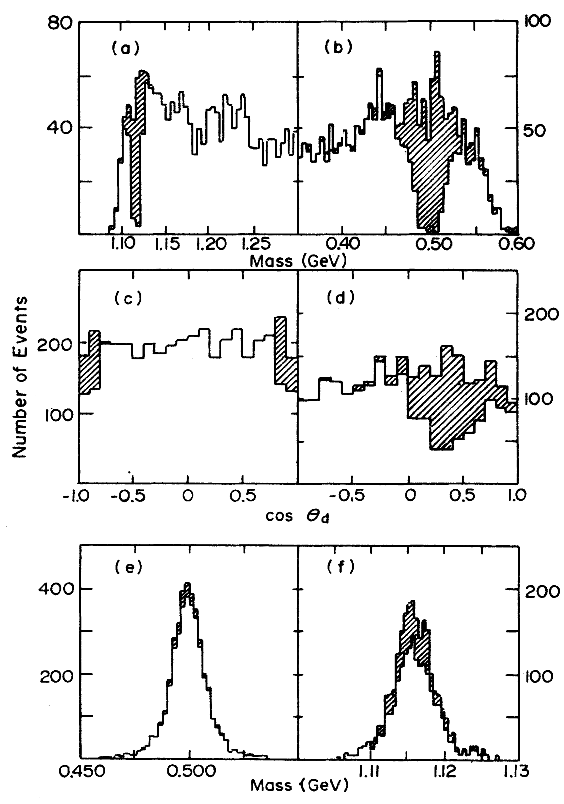

FIG. 1. (a), (b), (e), (f). Effective-mass distributions $M(A^+B^-)$ of V^0 decay products where A^+ and B^- are assumed to be (a) $p\pi^-$ and (e) $\pi^+\pi^-$ in events with K_S^0 fits; and (b) $\pi^+\pi^-$ and (f) $p\pi^-$ in events with Λ fits. Distributions in $\cos\theta_d$ (see text) are given in (c) for K_S^0 events and in (d) for Λ events. The unshaded areas denote unambiguous events, while the shaded areas refer to the ambiguous events assigned to K_S^0 or Λ as described in text.

was called a K^0_S if

$$\chi^2(\text{as } K^0_S) < 2.0\chi^2(\text{as } \bar{\Lambda}).$$

For K^0_S/Λ ambiguities, the V^0 was called a Λ if

$$\chi^2(\text{as } \Lambda) < 1.9\chi^2(\text{as } K^0_S).$$

The shaded events in Figs. 1(a) and 1(b) represent the ambiguous events assigned by this method; using the algorithm does result in smooth distributions with the dips filled in. Moreover, the number of $K^0_S/\bar{\Lambda}$ ambiguities assigned to K^0_S by this technique is roughly equal to the number of K^0_S/Λ ambiguities assigned to K^0_S, as is expected from the symmetry of the K^0_S decay. A further check on the method used to resolve ambiguities is shown in Figs. 1(c) and 1(d), which give the distributions of events with respect to θ_d, the angle between one of the V^0 decay products and the incoming V^0 direction in the V^0 rest frame. The assigned ambiguous events (the shaded areas) fill in the dips in these distributions and result in distributions which are consistent with isotropy. As can be seen from Figs. 1(e) and 1(f), assigning the correct masses to the decay particles results in invariant mass distributions for the K^0 and Λ that peak at 498 and 1116 MeV with widths of 16 and 6 MeV, respectively, indicating good experimental resolution. The final numbers of V^0 fits after resolving the ambiguities are given in Table I.

To compensate for V^0's which leave the chamber before decaying or decay within 0.5 cm of the primary vertex, weights were calculated in the conventional way. The average weights for K^0_S, Λ, and $\bar{\Lambda}$ were 1.13, 1.13, and 1.18, respectively; the numbers of weighted events are shown in Table I.

III. CROSS SECTIONS AND INCLUSIVE DISTRIBUTIONS OF K^0_S, Λ, AND $\bar{\Lambda}$

In calculating the cross sections further corrections have been made for detection, measuring, and fitting losses, as well as for the neutral decay modes of the strange particles. The μb/event value used for these cross sections has been previously determined.[5] The total inclusive cross sections for reactions (1)–(7) are given in Table II together with the cross sections as functions of the charged multiplicity of the production vertex. All errors quoted in this work are purely statistical. Systematic errors, which have not been included, have been estimated to be 5%, 5%, and 10% for K^0_S, Λ, and $\bar{\Lambda}$, respectively.

In Fig. 2 the cross sections for $\pi^- p \to K^0_S + X$ and $\pi^- p \to \Lambda + X$ obtained in this experiment are compared with cross sections for reactions (1) and (2) from previous studies[1,2,6,7] as a function of the

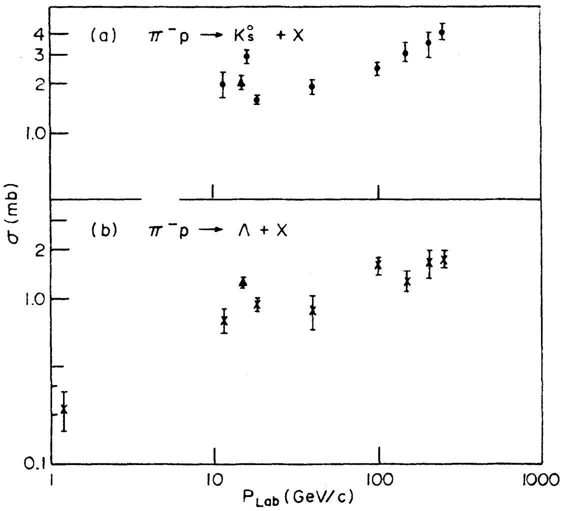

FIG. 2. Cross sections for (a) $\pi^- p \to K^0_S + X$ and (b) $\pi^- p \to \Lambda + X$ as a function of the incident π^- laboratory momentum. Results of this experiment are shown with triangles.

incoming π^- lab momentum.

The ratios of the topological cross sections for reactions (1)–(3) to the total inelastic $\pi^- p$ cross section at 15 GeV/c (Ref. 6) are presented in Fig. 3. The topological cross sections for K^0_S and Λ inclusive production are seen to be largest for four-prong events, and the cross section for reaction (1) is higher than the cross section for reaction (2) in all topologies. The cross section for $\bar{\Lambda}$ inclusive production, which involves baryon-

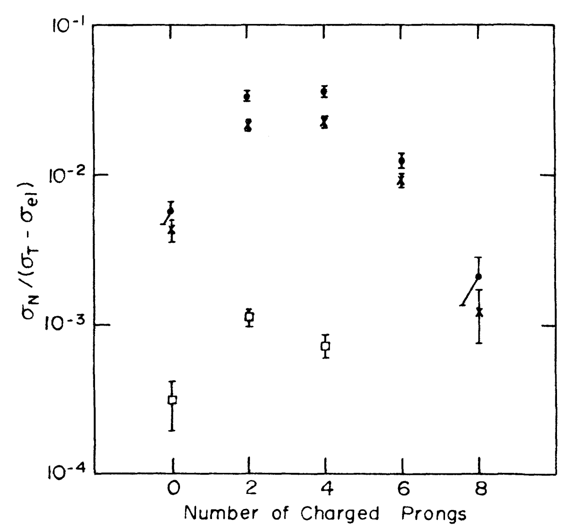

FIG. 3. Fractions of the total inelastic $\pi^- p$ cross section ($\sigma_T - \sigma_{el}$) as a function of the number of charged prongs for production of K^0_S (circles), Λ (crosses), and $\bar{\Lambda}$ (squares).

TABLE II. Neutral strange particles, inclusive cross sections in μb for $\pi^- p \to K_S^0 + X$, $\Lambda + X$, $\bar{\Lambda} + X$, $K_S^0 K_S^0 + X$, $K_S^0 \Lambda + X$, $\Lambda\bar{\Lambda} + X$, and $K_S^0 \bar{\Lambda} + X$.

No. of charged secondaries	K_S^0	Λ	$\bar{\Lambda}$	$K_S^0 K_S^0$	$K_S^0 \Lambda$	$\Lambda\bar{\Lambda}$	$K_S^0 \bar{\Lambda}$
0	122.5 ± 22.4	92.5 ± 16.8	6.6 ± 2.5	17.0 ± 6.0	38.9 ± 11.7	5.3 ± 2.9	1.1 ± 1.1
2	713.6 ± 43.7	465.9 ± 30.0	23.9 ± 3.6	74.5 ± 9.6	117.8 ± 13.8	7.9 ± 2.6	3.1 ± 1.8
4	787.2 ± 48.8	479.7 ± 31.3	15.8 ± 3.0	52.5 ± 7.9	76.7 ± 10.4	5.3 ± 2.4	···
6	266.3 ± 29.1	199.5 ± 22.6	1.2 ± 0.8	6.6 ± 2.8	22.7 ± 5.8	1.1 ± 1.1	···
8	45.2 ± 15.7	26.6 ± 10.1	0.8 ± 0.8	4.2 ± 4.2	···	···	···
10	2.4 ± 1.6	1.8 ± 1.5	···	···	···	···	···
Total inclusive	1937.2 ± 76.7	1266.0 ± 52.7	48.3 ± 5.4	154.8 ± 15.0	256.1 ± 21.6	19.6 ± 4.7	4.2 ± 2.2

antibaryon pair production, is much smaller than those for K_S^0 and Λ production and peaks at a lower charge multiplicity than those for reactions (1) and (2). A large fraction of the $\bar{\Lambda}$'s are seen to be produced as part of $\Lambda\bar{\Lambda}$ pairs (see Table II).

Table III lists the ratios

$$\langle n_{V^0}\rangle^N = \frac{\sigma(\pi^- p \to V^0 + X)_{N\text{prongs}}}{\sigma(\pi^- p \to N\text{prongs})}, \tag{12}$$

where the overall $\pi^- p$ topological cross sections are taken from Ref. 6. It can be seen that K_S^0 production represents a larger fraction of the total $\pi^- p$ inelastic cross section within each topology than does Λ production. At higher multiplicities (above eight prongs) $\langle n_K\rangle^N$ and $\langle n_\Lambda\rangle^N$ become comparable within the uncertainties.

The average multiplicities of charged particles produced in reactions (1) and (2), $\langle n\rangle_{K_S^0}$ and $\langle n\rangle_\Lambda$, are

$$\langle n\rangle_{K_S^0} = 3.37 \pm 0.13, \tag{13}$$

$$\langle n\rangle_\Lambda = 3.36 \pm 0.15. \tag{14}$$

Thus, the average charged multiplicities are equal for both samples, and smaller than the overall $\pi^- p$ average charged multiplicity of $\langle n\rangle \sim 4.1$ at 15 GeV/c.[6]

Figure 4 shows the differential cross sections for reactions (1)–(3) as a function of the overall center-of-mass production angle θ^*. The K_S^0 distribution [Fig. 4(a)] has more events (~65% of the total) produced in the forward hemisphere. The corresponding distribution for Λ [Fig. 4(b)] shows a very strong backward peak, suggesting that most of the Λ's are produced in the target region.

The values of the asymmetry parameter $A = (F - B)/(F + B)$, where F (B) denotes the number of V^0's produced in the forward (backward) hemisphere, are given in Table IV as a function of topology. The asymmetry parameters for both K_S^0 and Λ are largest for events with no charged prongs, decreasing in absolute value as the number of charged prongs increases. The magnitude of the asymmetry parameter for Λ production is consistently higher than for K_S^0 production meaning that within each topology the Λ's are more peripherally produced than the K_S^0.

Figure 5 shows the inclusive distributions for K_S^0, Λ, and $\bar{\Lambda}$ of the invariant cross section

$$F(x) = \frac{2E^*}{\pi\sqrt{s}} \int \frac{d^2\sigma}{dx\,dP_T^2}\,dP_T^2,$$

where $x = P_L^*/P_{\max}^*$, P_L^* is the longitudinal momen-

TABLE III. Ratios between topological cross sections for K_S^0 and Λ production and the $\pi^- p$ topological cross sections at 15 GeV/c. The values of $\sigma(\pi^- p \to N$ prongs) at 15 GeV/c have been interpolated from data given in Ref. 6.

N (No. of charged prongs)	$\langle n_K\rangle^N = \dfrac{\sigma(\pi^- p \to K_S^0 X)_{N\text{ prongs}}}{\sigma(\pi^- p \to N\text{ prongs})}$	$\langle n_\Lambda\rangle^N = \dfrac{\sigma(\pi^- p \to \Lambda X)_{N\text{ prongs}}}{\sigma(\pi^- p \to N\text{ prongs})}$
2[a]	0.132 ± 0.018	0.086 ± 0.012
4	0.086 ± 0.006	0.054 ± 0.004
6	0.055 ± 0.006	0.041 ± 0.005
8	0.033 ± 0.010	0.020 ± 0.008
10	0.012 ± 0.008	0.009 ± 0.007

[a] The inelastic $\pi^- p \to$ (2 prongs) cross section was used in the calculation.

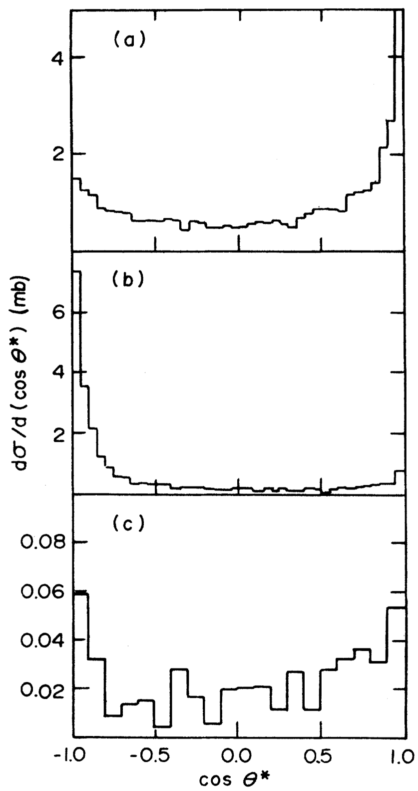

FIG. 4. Distributions of the cosine of the overall c.m. production angle θ^* for the (a) K^0's, (b) Λ, and (c) $\bar{\Lambda}$.

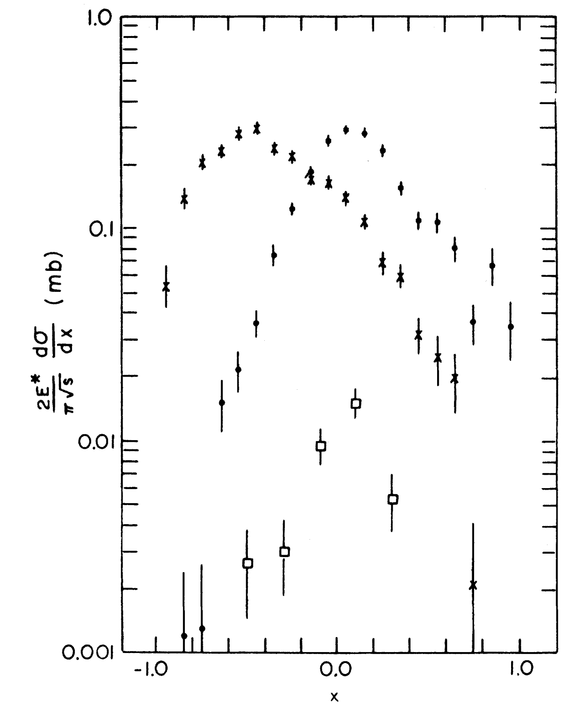

FIG. 5. Distributions of $(2E^*/\pi\sqrt{s})$ $(d\sigma/dx)$ as a function of x for K_S^0 (circles), Λ (crosses), and $\bar{\Lambda}$ (squares).

tum in the overall c.m. system and $P^*_{\max}$ is the maximum c.m. momentum allowed by kinematics. E^* is the center-of-mass energy of the produced particle, and $\sqrt{s}$ is the total center-of-mass energy. The K_S^0 distribution shows a slight excess in the positive x region; it is broad and peaked at $x \sim 0.1$. The shoulder close to $x = 1$ is due to the contribution from zero- and two-prong events. In contrast to the K_S^0 (and as already suggested by the $\cos\theta^*$ distribution), the Λ's are produced primarily in the negative x region, with the distribution peaking at $x \sim -0.5$. The invariant $F(x)$ distributions for both K_S^0 and Λ are very similar to those reported by $\pi^{\pm}p \to V^0 + X$ experiments at nearby energies.[1,7]

Figure 6 shows the differential cross sections $(1/\pi)(d\sigma/dy)$; the center-of-mass rapidity is defined as

$$y = \frac{1}{2}\ln\frac{E^* + P^*_L}{E^* - P^*_L}\,.$$

These distributions reveal very much the same information as do the $F(x)$ distributions, although the details of the central region are more evident.

All of the distributions shown in Figs. 4–6 are consistent with the hypothesis that the K_S^0 are produced more abundantly in the beam fragmentation region, but with non-negligible amounts being produced in the central and target fragmentation re-

TABLE IV. Asymmetry parameter A.

N (No. of charged prongs)	K_S^0	Λ	$\bar{\Lambda}$
0	0.43 ± 0.08	-0.75 ± 0.07	0.59 ± 0.32
2	0.30 ± 0.04	-0.67 ± 0.03	0.27 ± 0.20
4	0.20 ± 0.03	-0.52 ± 0.04	-0.06 ± 0.25
6	0.18 ± 0.06	-0.39 ± 0.07	...
8	0.09 ± 0.15	-0.15 ± 0.19	...
All topologies	0.25 ± 0.02	-0.56 ± 0.02	-0.15 ± 0.14

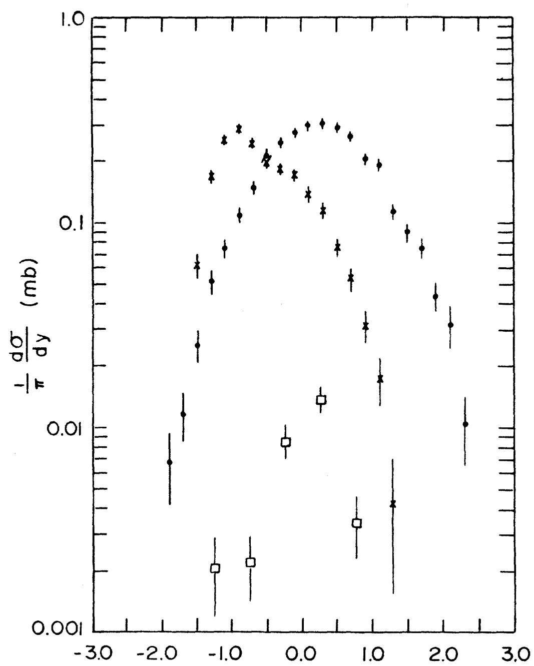

FIG. 6. Distribution of $(1/\pi)$ $(d\sigma/dy)$ as a function of y for K_S^0 (circles), Λ (crosses), and $\bar{\Lambda}$ (squares).

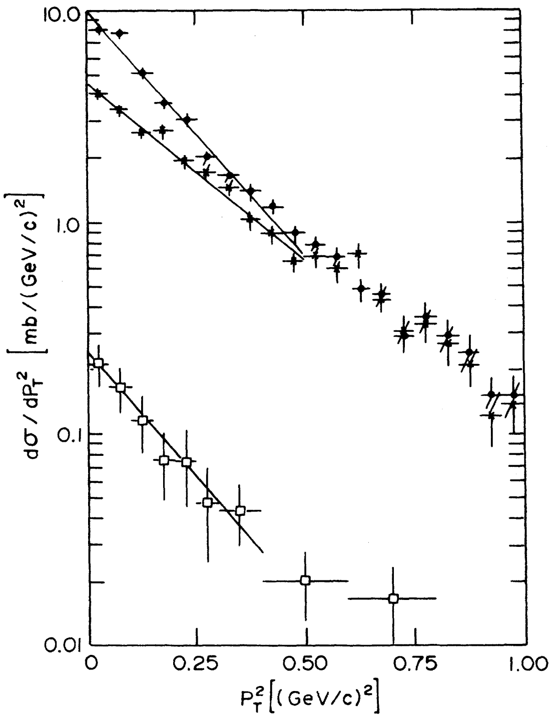

FIG. 7. $d\sigma/dP_T^2$ as a function of P_T^2 for K_S^0 (circles), Λ (crosses), and $\bar{\Lambda}$ (squares). The solid lines represent fits to the function $Ae^{-BP_T^2}$ (see Table V for values of the parameters A and B).

gions. The Λ particles are mostly produced in the target fragmentation region. The small number of $\bar{\Lambda}$ events makes it difficult to draw conclusions about such production, but it appears that there is no strong tendency for $\bar{\Lambda}$'s to be produced in association with either the beam or target fragmentation regions.

The transverse-momentum (P_T) distributions $d\sigma/dP_T^2$ for reactions (1)–(3) are shown in Fig. 7. For small P_T^2 values [i.e., below 0.5 (GeV/c)^2 for K_S^0 and Λ, and below 0.4 (GeV/c)^2 for $\bar{\Lambda}$ production], $d\sigma/dP_T^2$ can be parametrized by a function of the form $Ae^{-BP_T^2}$. The results of such fits are given in Table V and shown as solid lines in Fig. 7. At values of $P_T^2 > 0.5$ (GeV/c)^2, $d\sigma/dP_T^2$ for K_S^0 changes its slope so that it closely follows the Λ distribution. This feature has also been noted in $\pi^+p \to K_S^0 + X$ at 16 GeV/c (see Bosetti *et al.*, Ref. 1) and is discussed in more detail in Sec. V. The average transverse-momentum $\langle P_T \rangle$ values for each topology and for the total samples are given in Table VI.

The average charged multiplicities $\langle n_x \rangle$ of the charged particles produced with a K_S^0 [reaction (1)] and with a Λ [reaction (2)] are shown in Fig. 8(a) as a function of $\ln M_x^2$, where M_x is the invariant mass recoiling against the V^0. In order to select those events in which the Λ's are associated with the target proton and the K_S^0's with the incident π^-, only Λ events with $\cos\theta^* < -0.5$ (70% of the sample) and K_S^0 events with $\cos\theta^* > 0.5$ (46%) have been included. The two distributions are seen to be quite parallel, with the average charged multiplicity $\langle n_x \rangle$

TABLE V. Parameters for the fits $d\sigma/dP_T^2 = Ae^{-BP_T^2}$.

Reaction	P_T^2 range for fit [(GeV/c)^2]	A [mb/(GeV/c)^2]	B [(GeV/c)$^{-2}$]
$\pi^-p \to K_S^0 + X$	0–0.5	9.95 ± 0.59	5.34 ± 0.27
	0.5–1		3.70 ± 0.27
$\to \Lambda + X$	0–0.5	4.56 ± 0.20	3.83 ± 0.19
$\to \bar{\Lambda} + X$	0–0.4	0.24 ± 0.02	5.35 ± 0.49

TABLE VI. Average transverse-momentum values in $\pi^- p \to K_S^0 + X$ and $\pi^- p \to \Lambda + X$.

N (No. of charged prongs)	$\langle P_T \rangle$ (GeV/c) K_S^0	Λ
0	0.479 ± 0.022	0.433 ± 0.023
2	0.438 ± 0.006	0.507 ± 0.009
4	0.411 ± 0.006	0.480 ± 0.008
6	0.382 ± 0.010	0.460 ± 0.017
8	0.410 ± 0.035	0.540 ± 0.056
All topologies	0.421 ± 0.004	0.485 ± 0.006

being consistently higher for Λ events than for K_S^0 events at the same M_x^2 values. Moreover, for $M_x^2 \gtrsim 6$ (GeV)^2 the two distributions are well described by straight lines. A fit to the expression

$$\langle n_X \rangle = A + B \ln M_x^2 \tag{15}$$

yields slopes B of 1.64 ± 0.14 and 1.97 ± 0.13 for the Λ and K_S^0 distributions, respectively. These two values are comparable within errors with other

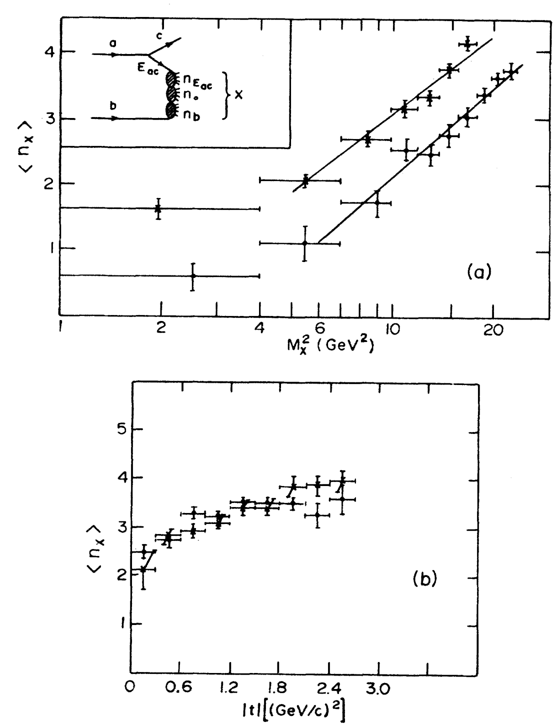

FIG. 8. Average charged multiplicity $\langle n_X \rangle$ as a function of M_X^2 (see text) for inclusive production of K_S^0 (circles) and Λ (crosses). The insert shows the diagram considered by the model described in Sec. III. (b) Average charged multiplicity $\langle n_X \rangle$ as a function of t_{π^-, K_S^0} for inclusive K_S^0 production (circles) and $t_{p, \Lambda}$ for inclusive Λ production (crosses). For selection of events in (a) and (b) see text.

values of B obtained in similar fits at higher energies and in different reactions[2,8] in agreement with predictions of various theoretical diffractive and multiperipheral models[9] which claim that B should be independent of energy and type of reaction. The same models also predict that the coefficient of $\ln M_x^2$ should be independent of the four-momentum transfer squared (t) and, within the uncertainties, the slopes B obtained in the present experiment for both Λ and K_S^0 are found not to depend on t.

Although the slope B is independent of t in the region in which $\langle n_X \rangle$ is linear in $\ln M_X^2$, the intercept A has a t dependence. This results in the overall dependence of $\langle n_X \rangle$ on t shown in Fig. 8(b), which includes only those events from Fig. 8(a) with $M_X^2 > 6$ (GeV)^2. As one can see from Fig. 8(b), the distributions for Λ and K_S^0 are very similar within the uncertainties both in shape and in absolute magnitude.

All the above features of $\langle n_X \rangle$ can be analyzed within the framework of a simple model that has been proposed[10] to calculate $\langle n_X \rangle$ for any inclusive reaction of the type $a + b \to c + X$. One assumes that the outgoing particles can originate from three distinct regions [see insert in Fig. 8(a)]: the region in which particle b fragments into n_b particles on the average (n_b depends only on the nature of particle b), a central region in which an average of n_0 particles are produced independent of the nature of a, b, and c, and the region in which the exchanged particle E_{ac} fragments on the average into $n_{E_{ac}}$ particles. According to this model $n_{E_{ac}}$ might be a function of s/M_X^2 and t. Then $\langle n_X \rangle$ can be written as

$$\langle n_X \rangle = n_{E_{ac}} + n_0 + n_b . \tag{16}$$

For sufficiently high values of M_X^2 (the lower limit cannot be exactly specified by this model) n_0 is expected to have the form $B \ln M_X^2$ where B is a constant, independent of s and reaction type. Applying this model to production of Λ's associated with the proton vertex and K_S^0's associated with the incident π^- one can write

$$\langle n_X \rangle_\Lambda = n_{E_{p\Lambda}} + n_0 + n_\pi , \tag{17}$$

$$\langle n_X \rangle_{K_S^0} = n_{E_{\pi^- K_S^0}} + n_0 + n_p , \tag{18}$$

where $n_{E_{p\Lambda}}$ and $n_{E_{\pi^- K_S^0}}$ are the multiplicities associated with the exchanged particles. The difference between the multiplicities for Λ and K_S^0 production is therefore

$$\langle n_x \rangle_\Lambda - \langle n_x \rangle_{K_S^0} = (n_{E_{p\Lambda}} - n_{E_{\pi^- K_S^0}}) + (n_\pi - n_p) . \tag{19}$$

The average result obtained for this difference from Fig. 8(a) (for $M_X^2 > 6$ GeV^2) is 0.90 ± 0.15.

Since n_π and n_p are not supposed to depend on energy, one can take for $n_\pi - n_p$ the value of 0.55 ±0.05 reported at 147 GeV/c.[8] This yields

$$n_{E_{p\Lambda}} - n_{E_{\pi^- K^0_S}} = 0.35 \pm 0.16\,. \tag{20}$$

One might expect $n_{E_{p\Lambda}}$ to be different from $n_{E_{\pi^- K^0_S}}$ because (a) the exchanged objects E are coupled to different particles in Λ production than in K^0_S production, and (b) different exchange particles contribute in Λ production than in K^0_S production. For example, only a virtual object having the K^*-quantum numbers can be responsible for K^0_S production, whereas for Λ production both K^+ and K^{*+} can contribute.

It is interesting to note that the difference (19) is almost constant for the entire $\ln M_x^2$ interval for $M_x^2 > 6$ GeV^2, suggesting similar s/M_x^2 and t dependence of $n_{E_{p\Lambda}}$ and $n_{E_{\pi^- K^0_S}}$ since $n_\pi - n_p$ is expected to be constant.

An interesting comparison can be made with results from an experiment at 147 GeV/c,[8] which found

$$n_{E_{pp}} - n_{E_{\pi\pi}} = 0.34 \pm 0.13\,. \tag{21}$$

Comparing (20) and (21), it appears that a virtual object coupled to two baryons fragments on the average into more charged particles than does a virtual object coupled to two mesons. However, more experimental evidence is needed to confirm this result.

IV. Λ POLARIZATION AND TRIPLE-REGGE ANALYSIS OF Λ INCLUSIVE PRODUCTION

The polarization of the Λ's produced in reaction (2) is shown in Fig. 9(a) as a function of the four-momentum transfer squared from the target proton to the Λ hyperon. The Λ polarization is defined as follows:

$$P \pm \delta P = \frac{3}{\alpha N}\sum_{i=1}^{N}(\hat{u}_i \cdot \hat{n}_i) \pm \tfrac{1}{2}\left[\frac{3-(\alpha P)^2}{N}\right]^{1/2}, \tag{22}$$

where $\hat{u}_i$ is a unit vector along the direction of the decay proton in the Λ rest frame, $\hat{n}_i$ is a unit vector normal to the plane of the Λ and the incident pion, and N is the number of observed Λ's. The decay parameter α is taken to be $\alpha = 0.65$. In most of the $|t|$ intervals considered, the values of the Λ polarization are small and negative, and the average polarization in the interval $0 \le |t| \le 1$ (GeV/c)^2 is -0.134 ± 0.095.

Figures 9(b)–9(d) show the dependence of the Λ polarization on x and P_T. A recent study[11] of Λ polarization in the target fragmentation region [de-

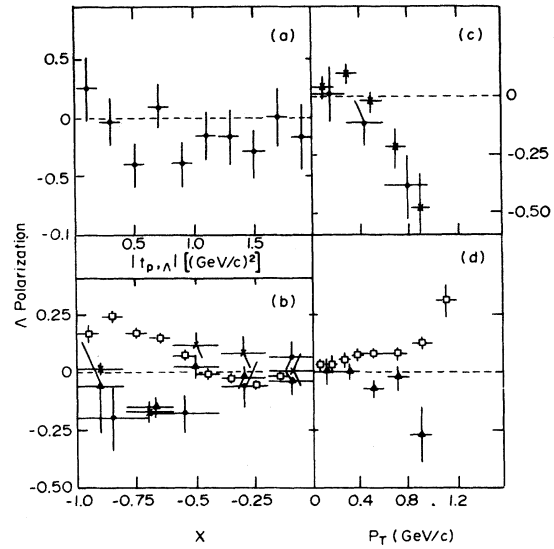

FIG. 9. Polarization of Λ in various inclusive reactions as a function of (a) t, the four-momentum transfer from the target proton to the Λ, (b) x, the Feynman variable, (c) and (d) P_T, the transverse momentum, for events with $x(\Lambda) \le -0.2$; circles: $\pi^- p \to \Lambda + X$ (this experiment), squares: $K^- p \to \Lambda$+pions at 4.2 GeV/c Ref. 11, triangles: $K^- p \to \Lambda + K\bar{K}$+pions at 4.2 GeV/$c$, Ref. 11, crosses: $\bar{p}p \to \Lambda + X$ at 5.7 GeV/c, Ref. 11.

fined by $x(\Lambda) < -0.2$] points out that the dependence of the polarization on x and P_T differs markedly in various inclusive reactions, depending on whether the production is via strangeness-annihilating or strangeness-nonannihilating processes. Reaction (2) is a strangeness-nonannihilating process and indeed the Λ polarization as a function of x and P_T exhibits behavior very similar to that observed in other strangeness-nonannihilating processes such as $Kp \to \Lambda K\bar{K}$+pions at 4.2 GeV/c[11] and $\bar{p}p \to \Lambda + X$ at 5.7 GeV/c.[11] All of these reactions are characterized by a small negative polarization for $x < -0.5$ [see Fig. 9(b)], and by a negative polarization that increases in magnitude with increasing P_T [see Figs. 9(c) and 9(d)]. In contrast, the strangeness-annihilating process $K^- p \to \Lambda$ + pions at 4.2 GeV/c[11] exhibits a distinctly positive Λ polarization for $x < -0.5$ [see Fig. 9(b)], and a positive polarization which increases with P_T [see Fig. 9(d)].

Since most of the Λ's [reaction (2)] are produced in the proton fragmentation region, one can try to analyze the data in the framework of the triple-Regge model. The diagram for this process is shown in Fig. 10. The Regge trajectory $\alpha_K(t)$ refers to K or K^* exchange whereas $\alpha_M(0)$ denotes the Pomeron or meson exchange intercept. The differential cross section may then be expressed as

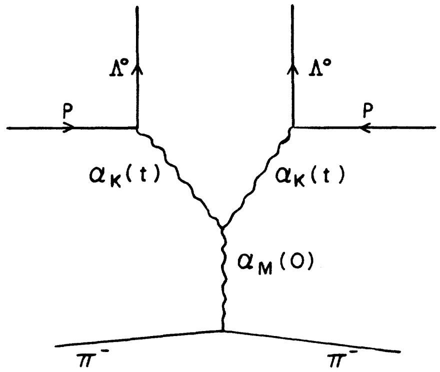

FIG. 10. Triple-Regge diagram for Λ production in $\pi^- p$ interactions.

$$\frac{d^2\sigma}{dt\,d(M_X{}^2/s)}=G_{KKM}(t)\left(\frac{M_X{}^2}{s}\right)^{1-2\alpha_K(t)}(M_X{}^2)^{\alpha_M(0)-1}\,. \tag{23}$$

Therefore, at a given s value,

$$\frac{d^2\sigma}{dt\,dM_X{}^2}=G'(t)(M_X{}^2)^{\alpha_M(0)-2\alpha_K(t)}\,. \tag{24}$$

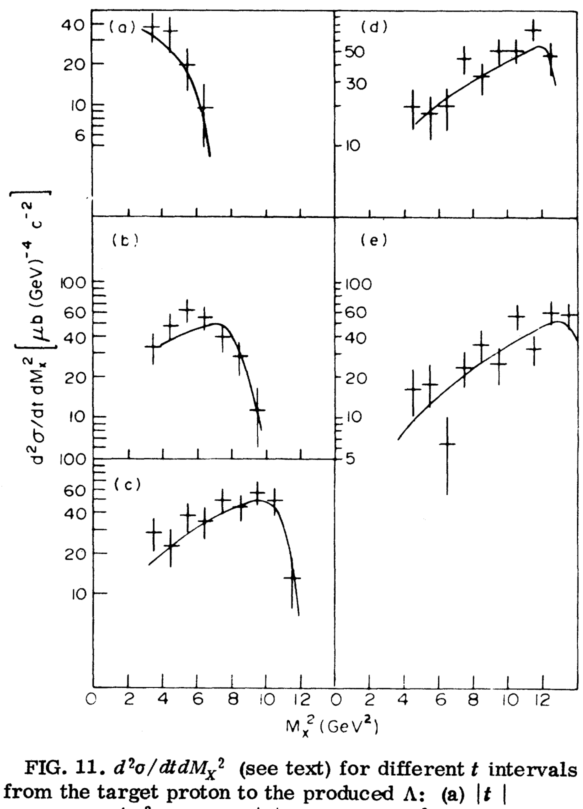

FIG. 11. $d^2\sigma/dt\,dM_X{}^2$ (see text) for different t intervals from the target proton to the produced Λ: (a) $|t| \leq 0.2$ (GeV/c)^2, (b) $0.2<|t|\leq 0.4$ (GeV/c)^2, (c) $0.4<|t| \leq 0.6$ (GeV/c)^2, (d) $0.6<|t|\leq 0.8$ (GeV/c)^2, (e) $0.8<|t| \leq 1.0$ (GeV/c)^2. Solid lines are the results of a triple-Regge model fit (see text).

Figure 11 shows $d\sigma/dM_X{}^2$ for several t intervals (where t is defined from the proton target to the Λ). The data have been fitted to the following expression:

$$\frac{d^2\sigma}{dt\,dM_X{}^2}=Ae^{Bt}(M_x{}^2)^{C(t)}\,, \tag{25}$$

where

$$C(t)=\alpha_M(0)-2\alpha_K(0)-2\alpha'_K\cdot t$$

taking properly into account[13] the effects of the kinematic limit on the upper end of the $M_X{}^2$ distributions. To ensure the validity of the diagram in Fig. 10, only events with $|t|\leq 1$ GeV/c^2 and $M_X{}^2 \geq 3$ GeV^2 have been considered. Furthermore, $\Lambda\pi^+$ combinations with effective mass $1.34 \leq M(\Lambda\pi^+) \leq 1.42$ GeV have been rejected to eliminate Λ's produced as $\Sigma^+(1385)$ decay products. The fitted curves are shown as solid lines in Fig. 11 and the values obtained for the fitted parameters are

$$\begin{aligned}&\alpha_M(0)-2\alpha_K(0)=0.17\pm0.15\,,\\&\alpha'_K=0.90\pm0.15\,,\\&A=60.0\pm12.5\,,\\&B=5.1\pm0.6\,.\end{aligned} \tag{26}$$

The intercept $\alpha_M(0)$ represents contributions from both Pomeron and Reggeon trajectories. The weak dependence of the cross section for reaction (2) on the incident π^- momentum (see Fig. 2), and the fact that the overall Λ polarization is small in this experiment as in other strangeness-nonannihilating processes,[14] suggest the possibility of Pomeron dominance. If one therefore assumes $\alpha_M(0)$ to be the Pomeron intercept [i.e., $\alpha_M(0)\sim 1.0$], the intercept of the effective K trajectory is found to be $\alpha_K(0)\sim 0.4$, which is compatible with the accepted value for the K^* intercept [$\alpha_{K^*}(0)\sim 0.3$]. However, this value of $\alpha_K(0)\sim 0.4$ is highly dependent on the assumptions one makes about Pomeron dominance and the value of the Pomeron intercept.

V. K^* (890) AND Σ(1385) INCLUSIVE PRODUCTION

The $K_S^0\pi$ and $\Lambda\pi$ effective-mass distributions are shown in Figs. 12(a)–12(d). In calculating the effective masses, the fitted values of the V^0 momenta and the measured pion momenta have been used.

The $K_S^0\pi^+$ mass distribution [Fig. 12(a)] shows a clear, narrow peak at the mass of the K^*(890). The solid line in Figure 12(a) represents the results of a fit to a modified Breit-Wigner resonance shape[15] on top of a polynomial background. The mass and width of the K^*(890) used in the fit were $M_0=892$ MeV and $\Gamma_0=50$ MeV as tabulated in Ref. 16. The resulting cross section is

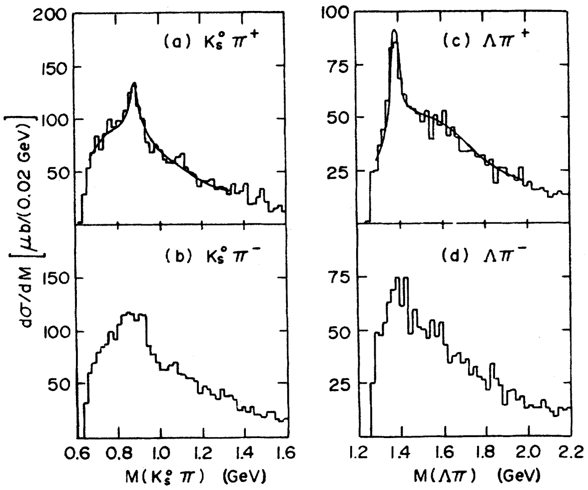

FIG. 12. Effective-mass distributions of (a) $K_S^0\pi^+$, (b) $K_S^0\pi^-$, (c) $\Lambda\pi^+$, and (d) $\Lambda\pi^-$. Solid lines in (a) and (c) are results of fits (see text). All possible combinations have been included, multiplied by the appropriate cross section/event factor.

$$\sigma(\pi^-p \to K^{*+}(890) + X) = 195 \pm 35 \ \mu b . \qquad (27)$$
$$\hookrightarrow K_S^0\pi^+$$

By contrast, no narrow $K^*(890)$ peak is seen in the $K_S^0\pi^-$ mass distribution [Fig. 12(b)], and attempts to fit the distribution with the same parametrization as for the $K_S^0\pi^+$ effective mass histogram resulted in no acceptable fit. If one considers the π^-p reactions in which a K^0 or $\overline{K}^0$ may be produced, one sees that there are two general classes:

(a) Reactions in which a strange baryon (Λ or Σ) is produced, so that K^0 or K^+ (and not $\overline{K}^0$) may also be produced to conserve strangeness.

(b) Reactions in which a nonstrange baryon is produced, so that both K^0 and $\overline{K}^0$ may result, either together in pairs or with charged kaons.

Thus, there are more ways to produce a K^0 than a $\overline{K}^0$ in π^-p interactions. It is difficult to estimate the relative amounts of K^0 and $\overline{K}^0$ production at 15 GeV/c since the only data on exclusive K^0 and $\overline{K}^0$ production in π^-p interactions exist at ~4 GeV/c and below.[6] Still, a very crude extrapolation of the existing low-energy cross sections gives a ratio of $K^0/\overline{K}^0 \gtrsim 2$, thus providing a possible explanation for the lack of K^{*-} (890) produced as compared to K^{*+}(890).

No higher-mass K^*'s have been observed in the $K_S^0\pi$ or $K_S^0\pi\pi$ effective-mass distributions.

The effective-mass distribution of the $\Lambda\pi^+$ [Fig. 12(c)] looks very different from that of the $\Lambda\pi^-$ [Fig. 12(d)]. While a strong Σ^+(1385) signal is present in the $\Lambda\pi^+$ distribution, no clear evidence for resonant structure is seen in the $\Lambda\pi^-$ mass plot, consistent with the observation (see Sec. III) that the Λ's are produced primarily at the proton vertex.

The $\Lambda\pi^+$ mass distribution has been fitted with a similar parametrization as the one used for $K_S^0\pi^+$, taking for the mass and width of the Σ(1385) the values $M_0 = 1383$ MeV and $\Gamma_0 = 35$ MeV.[16] The result is shown as the solid line in Fig. 12(c), and the corresponding cross section for inclusive Σ^+(1385) production is

$$\sigma(\pi^-p \to \Sigma^+(1385) + X) = 174 \pm 25 \ \mu b . \qquad (28)$$
$$\hookrightarrow \Lambda\pi^+$$

In order to study the inclusive production of K^{*+}(890) and Σ^+(1385) as a function of their center-of-mass rapidity (y) and transverse momentum squared (P_T^2), the $K_S^0\pi^+$ and $\Lambda\pi^+$ effective mass distributions were obtained for different ranges of y and P_T^2 of the two-particle systems. The distribution within each bin was then fitted as previously described in order to determine the resonance cross section for that bin. The resulting distributions are shown in Figs. 13(a)–13(d). The K^{*+}(890)

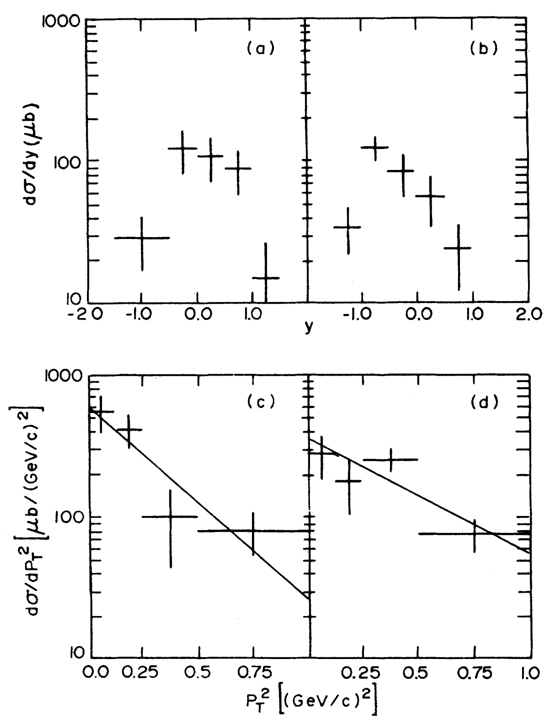

FIG. 13. Distributions of $d\sigma/dy$ as a function of y for (a) K^{*+}(890) and (b) Σ^+(1385) production. Distributions of $d\sigma/dP_T^2$ as a function of P_T^2 for (c) K^{*+}(890) and (d) Σ^+(1385) production. The solid lines in (c) and (d) represent fits to the function $Ae^{-BP_T^2}$ (see text).

and $\Sigma^+(1385)$ rapidity distributions [Figs. 13(a) and 13(b)] show features similar to those of K^0_S and Λ, respectively (Fig. 6): The $K^{*+}(890)$ is generally produced slightly forward in the center-of-mass frame, while the $\Sigma^+(1385)$ is produced predominantly backward.

The distributions in P_T^2 have been fitted to the expression $Ae^{-BP_T^2}$ over the range $0<P_T^2<1$ (GeV/c)^2, with the resulting slopes

$$B_{K^{*+}(890)} = 3.2 \pm 1.1\,,$$
$$B_{\Sigma^+(1385)} = 1.8 \pm 0.8\,. \quad (29)$$

The fits are shown as the solid lines in Figs. 13(c) and 13(d).

A recent study[17] has found that inclusively produced resonances and heavy particles seem to have a universal $d\sigma/dP_T^2$ slope of $B\sim 3.4$, independent of the initial state and over a range of incident beam momentum from 4 to 200 GeV/c. Lighter particles (pions and kaons) seem to have similar slopes if only the range $P_T^2 \gtrsim 1$ (GeV/c)^2 is considered. Below that point the slopes become steeper, with the additional cross section at small P_T^2 being attributed to resonance decay products. It has therefore been conjectured that directly produced particles have a universal slope.

As can be seen, the slope obtained in the present experiment for $K^*(890)$ production is perfectly consistent with this universal value. The slope for $\Sigma^+(1385)$ production is lower, but given the small $\Sigma^+(1385)$ cross section, it is difficult to make a more definite statement.

It is also worth noting that the slope for inclusive Λ production ($B = 3.83 \pm 0.19$) agrees reasonably well with the universal value, as expected for a heavy particle. The observed break in the K^0_S slope (see Sec. III) is also consistent with this universality; a fit to the $d\sigma/dP_T^2$ distribution over the range $0.5<P_T^2<1.0$ (GeV/c)^2 yields a slope of $B = 3.70 \pm 0.27$.

VI. SUMMARY AND CONCLUSIONS

The inclusive cross sections for neutral strange particles at 15-GeV/c incident π^- momentum are

$$\begin{aligned}
\sigma(\pi^-p \to K^0_S + X) &= (1937.2 \pm 76.7)\ \mu\text{b}\,,\\
\sigma(\pi^-p \to \Lambda + X) &= (1266.0 \pm 52.7)\ \mu\text{b}\,,\\
\sigma(\pi^-p \to \bar{\Lambda} + X) &= (48.3 \pm 5.4)\ \mu\text{b}\,,\\
\sigma(\pi^-p \to K^0_S\Lambda + X) &= (256.1 \pm 21.6)\ \mu\text{b}\,, \qquad (30)\\
\sigma(\pi^-p \to \Lambda\bar{\Lambda} + X) &= (19.6 \pm 4.7)\ \mu\text{b}\,,\\
\sigma(\pi^-p \to K^0_S K^0_S + X) &= (154.8 \pm 15.0)\ \mu\text{b}\,,\\
\sigma(\pi^-p \to K^0_S\bar{\Lambda} + X) &= (4.2 \pm 2.2)\ \mu\text{b}\,.
\end{aligned}$$

K^0_S production occurs more abundantly in the forward direction, while the Λ's are produced almost exclusively backward in the target fragmentation region. The $\bar{\Lambda}$'s are produced in the central region, largely in pairs with Λ's.

The average charged multiplicity $\langle n_X\rangle$ of the system recoiling against the Λ's is consistently higher for a given value of the system mass M_X than is the corresponding average charged multiplicity for the K^0_S. The $\langle n_X\rangle$ distributions obtained by considering only backward-going Λ's and forward-going K^0_S's are quite parallel and linear in $\ln M_X^2$ for $M_X^2>6$ GeV^2, and the difference between the multiplicities is almost constant in this M_X^2 range. The average difference $\langle n_X\rangle_\Lambda - \langle n_X\rangle_{K^0_S}$ for $M_X^2>6$ GeV^2 is 0.90 ± 0.15.

The polarization of Λ's produced in reaction (2) is small and negative in the target fragmentation region. Its dependence on x and P_T follows very closely the behavior of the Λ polarization measured in other strangeness-nonannihilating reactions at different energies and with different beams incident on protons. Assuming $\alpha_M(0)$ to be the Pomeron intercept, a triple-Regge-pole model fit to the differential cross section $d^2\sigma/dt\,dM^2$ for Λ production in the target fragmentation region yields an effective trajectory consistent with that of the K^*.

The cross sections for inclusive $K^{*+}(890)$ and $\Sigma^+(1385)$ production are

$$\begin{aligned}
\sigma(\pi^-p \to K^{*+}(890) + X) &= 195 \pm 35\ \mu\text{b}\,,\\
&\quad \searrow K^0_S\pi^+\\
\sigma(\pi^-p \to \Sigma^+(1385) + X) &= 174 \pm 25\ \mu\text{b}\,. \qquad (31)\\
&\quad \searrow \Lambda\pi^+
\end{aligned}$$

The $K^{*+}(890)$'s are found to be preferentially produced in the forward hemisphere, while the $\Sigma^+(1385)$ production occurs primarily in the target fragmentation region. These resonances have been found to have essentially exponential distributions in P_T^2. The slope of the $d\sigma/dP_T^2$ distribution of the $K^{*+}(890)$ is in good agreement with other observations of a universal slope of ~3.4 (GeV/c)$^{-2}$, although the $\Sigma^+(1385)$ is less steep. The slopes for the inclusive K^0_S [for $0.5<P_T^2<1$ (GeV/c)^2] and Λ distributions are also consistent with a value of ~3.4 (GeV/c)$^{-2}$.

ACKNOWLEDGMENTS

We wish to express our thanks to SLAC and especially to the 82-in. hydrogen bubble-chamber crew whose efforts made this experiment possible.

We also wish to thank the MIT PEPR scanning and measuring staff for their dedicated work in processing the film. This work is supported in part through funds provided by the U. S. Energy Research and Development Administration under Contract No. EY-76-C-02-3069*000. Also, one of us (J. E. B.) would like to thank the Fannie and John Hertz Foundation for financial support.

---

*On leave of absence from Tel-Aviv University, Israel.
†Present address: Tel-Aviv University, Israel.
‡Present address: The Weizmann Institute of Science, Israel.
[1]D. Crennell *et al.*, Phys. Rev. Lett. 28, 643 (1972); P. Borzatta *et al.*, Lett. Nuovo Cimento 7, 641 (1973); P. H. Stuntebeck *et al.*, Phys. Rev. D 9, 608 (1974); A. Pletnikov *et al.*, Yad. Fiz. 20, 937 (1974); [Sov. J. Nucl. Phys. 20, 496 (1975); O. Balea *et al.*, Nucl. Phys. B79, 57 (1974); P. Bosetti *et al.*, *ibid.* B94, 21 (1975).
[2]S. Kahn *et al.*, Bull. Am. Phys. Soc. 21, 87 (1976); T. Watts *et al.*, *ibid.* 21, 593 (1976); P. E. Stamer *et al.*, *ibid.* 22, 23 (1977).
[3]E. S. Hafen, MIT APC Programming Note No. DAS 75-1, 1975 (unpublished).
[4]O. I. Dahl, T. B. Day, F. T. Solmitz, and N. L. Gould, LRL Programming Note No. P-126, 1968 (unpublished).
[5]Pierre Caron Trepagnier, Ph.D. thesis, MIT, 1976 (unpublished).
[6]E. Bracci *et al.*, CERN/HERA Report No. 72-1, 1972 (unpublished).
[7]J. Whitmore, University of Michigan report, 1976 (unpublished) and references therein; J. Whitmore, Phys. Rep., 10C, 273 (1974).
[8]D. Fong *et al.*, Phys. Rev. Lett. 37, 736 (1976).
[9]W. R. Frazer and D. R. Snider, Phys. Lett. 45B, 136 (1973); C. F. Chan, Phys. Rev. D 8, 179 (1973).
[10]C. DeTar, private communication.
[11]Amsterdam-CERN-Oxford Collaboration, paper submitted to the International Conference on High Energy Physics, Tbilisi, CERN/EP/Phys. Report No. 76-25 (unpublished).
[12]C. E. DeTar *et al.*, Phys. Rev. Lett. 26, 675 (1971).
[13]S. N. Ganguli and B. Sadoulet, Nucl. Phys. B53, 458 (1973).
[14]R. D. Field, invited talk on physics with polarized targets, CALT Reports Nos. 68-559 and 68-446 (unpublished).
[15]J. D. Jackson, Nuovo Cimento 34, 1644 (1974).
[16]Particle Data Group, Rev. Mod. Phys. 48, S1 (1976).
[17]P. Schmid, in *Proceedings of the XVIII International Conference on High Energy Physics, Tbilisi*, 1976, edited by N. N. Bogoliubov *et al.* (JINR, Dubna, U.S.S.R., 1977), Vol. I, p. A2-9.